Taylor & Francis
Taylor & Francis Group

Synthesis of carbazole-based dendritic conjugated polymer: a dual channel optical probe for the detection of I⁻ and Hg²⁺

Yimin Wu, Ling Zhang, Fudong Ma, Tao Ding and Ablikim Obolda

College of Chemistry and Chemical Engineering, Xinjiang Agricultural University, Xinjiang, PR China

ABSTRACT

A new type of carbazole-based blue-emitting dendritic conjugated polymer, poly[(9,9-dioctyl)-2,7-fluorene-co-4,4′,4″-triphenylamine-co-9-(4-(9H-carbazol-9-yl)butyl)-3,6-carbazole](P), was successfully synthesized by Suzuki coupling reaction. Chemical structures of monomers and polymer were verified by FI-IR and ^{1}HNMR characterizations. We found that polymer showed a special selectivity and high sensitivity for I⁻. With the addition of I⁻, the fluorescent polymer solution was obviously quenched. The polymer showed a special detection effect on I⁻. However, the fluorescent polymer was obviously restored when Hg²⁺ was added to the P/I⁻ system due to the large complexation between I⁻ and Hg²⁺. The anti-interference experiments of probe P/I⁻ showed that other background cations have a slight influence on detecting Hg²⁺, and the calculated detection limit of Hg²⁺ reached 9.7×10^{-8} M, which could be a potential application for a two-channel cyclic detection of I⁻ and Hg²⁺. Additionally, it was found that the theoretical values were in agreement with the experimental data.

1. Introduction

In recent years, heavy metal pollution has drawn much attention due to its irreversible negative effect on human health and the environment. However, the still widely used heavy metals in the cosmetics, industrial, and material fields accumulate in living organism and cause vital diseases to humans and animals as well as pose a serious threat to the natural environment [1,2]. Among the various heavy metal ions, mercury ions and their derivatives are listed as the deadly toxins and pollutants among the 'precarious dangerous pollutants' [3]. In the human body, mercury is accumulated through the skin, respiratory tract, food, and so on, and can cause digestive system diseases, muscle weakness, nerve disorders, and kidney disease [4,5]. Therefore, there is an urgent need to develop a mercury ion detection that can be easily and quickly applied.

In the past few decades, researchers have developed several methods to detect Hg²⁺, such as atomic absorption spectrometry [6], inductively coupled plasma mass spectrometry [7], anodic stripping voltammetry [8], and so on. Although these traditional detection methods have good sensitivity and selectivity, they are expensive, time-consuming, complicated to operate and require professional operators, and not suitable for on-site detection. Therefore, after tremendous hard work from researchers, optical probe detection methods that can quickly and accurately detect metal ions in environmental and biological samples are coming out [9–15]. Recently, a novel La³⁺-BSA-AuNCs-based fluorescent probe was reported by Kailasa'group [16]. This probe can detect four divalent metal ions (Hg²⁺, Cu²⁺, Pb²⁺, and Cd²⁺) simultaneously and exhibit excellent performance. Wang's group reported a quinoline-based derivative and its application for a sensitive probe detection of Hg²⁺ and I⁻in biological fields [17]. Teng et al. reported green-emission carbon dots (CDs) as fluorescent off-on probes for the highly selective sensing Hg²⁺ and I⁻ [18].

Fluorescent conjugated polymers (CPs) are one of the optical probe organic materials [19–23], which show excellent sensitivity in ion recognition due to their optical signal amplification properties [24,25]. In 2020, Maimaiti yiminget al. designed and synthesized a pyrimidine group containing conjugated polymer, in which it showed excellent optical properties for specific recognition of Hg²⁺ and I⁻ [26]. Neha's group designed and synthesized a water-soluble polymer probe with a side chain containing rhodamine group, which was used to detect Hg²⁺ in water and living cells and carry out naked eye colorimetry (colorless to pink to purple) for Hg²⁺ [27].

The carbazole and its derivatives are an important class of nitrogen-containing heterocyclic compounds. It has a rigid molecular structure, good planarity, and

CONTACT Fudong Ma ✉ xjaumafud@163.com 🏢 College of Chemistry and Chemical Engineering, Xinjiang Agricultural University, Urumqi 830052 Xinjiang, PR China; Ablikim Obolda ✉ aobolda@126.com 🏢 College of Chemistry and Chemical Engineering, Xinjiang Agricultural University, Xinjiang, PR China

biocompatibility as well as excellent optical properties [28–30]. Moreover, carbazole has a remarkable feature, which is easy to functionalize and covalently connect with other molecules, so it is widely used as a building block in various fields [31–39]. Recently, it has been reported that carbazole and triphenylamine-based conjugated polymer probes have certain advantages in the detection of I^- and Hg^{2+} [40–42]. Wang's group reported carbazole and triazole-containing conjugated polymer as a visual and fluorometric probe for Hg^{2+} and I^- [43]. They showed excellent detection and recognition performance for Hg^{2+} and I^-. However, the dendritic fluorescent conjugated polymer probe containing the carbazole group has not been reported yet.

In this paper, a carbazole-based blue-emitting dendritic conjugated polymer, poly[(9,9-dioctyl)-2,7-fluorene-co-4,4',4''-triphenylamine-co-(9-(4-(9H-carbazol-9-yl)butyl)-3,6-carbazole] (P), was successfully synthesized by the Suzuki coupling reaction. The sensing properties of P were systematically investigated.

2. Experiment

2.1. Materials

Petroleum ether, toluene, tetrahydrofuran, and methylene chloride were all purchased from Tianjin Best Chemical Co., Ltd. Ethyl acetate was purchased from Tianjin Yongsheng Fine Chemical Co., Ltd. Methyl acrylate was purchased from Tianjin Guangfu Fine Chemical Research Institute. Potassium carbonate was purchased from Sinopharm Chemical Reagent Co., Ltd. Tetrabutylammonium bromide was purchased from Shanghai Shanpu Chemical Co., Ltd. The above organic solvents are of analytical grade. Tricyclohexylphosphorus and palladium acetate were purchased from Aldrich, USA. Tetrahydrofuran (THF) and toluene were distilled from sodium in the presence of benzophenone and degassed before use. 2,7-Bis(4,4,5,5-tetramethyl-1,3,2-dioxaborolan-2-yl)-9,9-dioctylfluorene (R4) was synthesized according to the reported literature [44], and the corresponding spectra of R4 are shown in Figures S1 to S4.

Solutions of F^-, Cl^-, Br^-, SO_4^{2-}, Ac^-, HCO_3^-, $H_2PO_4^-$, SCN^-, OH^-, NO_3^-, CO_3^{2-}, and I^- were prepared from their sodium salt; Solutions of Ag^+, Ni^+, Fe^{3+}, Cu^{2+}, Pb^{2+}, Al^{3+}, Mg^{2+}, Ca^{2+}, Zn^{2+}, Cd^{2+}, and Ba^{2+} were prepared from their nitrate salts. Hg^{2+} was prepared from its acetate salt.

2.2. Instruments

IR spectrum was recorded on an EQUINOX 55 FT-IR spectrometer with KBr pellets. ^{1}HNMR and ^{13}C NMR spectra were collected on a BRUKER AVANCE III spectrometer. Number-average (M_n) and weighted-average (M_w) molecular weights were determined by Waters GPC LC20AD. UV–visible absorption spectra were recorded on a SHIMADZU UV-2450 UV-vis spectrophotometer. PL spectra were recorded on RF-5301PC spectrophotometer and the test slit width was 5 nm × 5 nm. HRMS was recorded on Agilent qtof-6550.

All-electron DFT calculations have been carried out by the latest version of ORCA quantum chemistry software (Version 5.0.1) [45]. For geometry optimization calculations of S_1 structure, PBE0 functional [46] and the mixed basis set (SARC-DKH-TZVP basis set for I atom and the def2-SV (P) basis set for other atoms) were used, and the optimal S_1 geometry for each compound was determined [47,48]. The DFT-D3 dispersion correction with BJ-damping was applied to correct the weak interaction to improve the calculation accuracy [49,50]. The Conductor-like Continuum Polarization Model was used to account for the solvation effect of THF [51]. The excited states and Spin-Orbit Coupling (SOC) calculations were performed with B3LYP functional and the mixed basis set (SARC-DKH-TZVP basis set for I atom and DKH-def2-TZVP(-f) basis set for other atoms) [52].

2.3. Synthesis of 3,6-dibromocarbazole (M1)

Under nitrogen atmosphere, N-bromosuccinimide (3.92 g, 22 mmol) in dichloromethane (50 mL) was added by the drop to the carbazole mixture (1.67 g, 10 mmol) and SiO_2 (5 g, 83.2 mmol) in dichloromethane (100 mL). The reaction mixture was stirred at room temperature for 24 hours. After the reaction was complete, SiO_2 was filtered and the solvent was evaporated by a rotary evaporator, and the crude product was purified by column chromatography using toluene as eluent and dried under a vacuum to afford 1.86 g (65%) of white powder. M1 was characterized by FT-IR, NMR, and HRMS (Figure S5, Figure S6, Figure S7, and Figure S8). FT-IR (KBr, cm^{-1}): 3420, 1598 (N-H), 1041(C-N), 794(C-H). ^{1}H NMR (400 MHz, DMSO-d_6) δ 11.60 (s, 1H), 8.43 (d, J = 1.8 Hz, 2 H), 7.51 (dt, J = 21.5, 5.3 Hz, 4 H). ^{13}C NMR (100 MHz, DMSO-d_6) δ 139.30, 139.30, 129.13, 123.88, 123.68, 113.57, 111.54. HRMS(ESI) calcd. for [M]$^+$ 324.8925, found 324.8913.

2.4. Synthesis of 9-(4-bromobutyl)-9H-carbazole (M2)

Carbazole (2 g, 11.97 mmol) and tetrabutylammonium bromide (0.08 g, 0.25 mmol) were added to 20 mL of toluene and then NaOH (50 wt%, 16 mL) was added. After 30 min, the 1,4-dibromobutane (10 g, 46.32 mmol) was added slowly by an addition funnel, and the reaction was

refluxed for 16 hours under the protection of N_2. After being cooled to room temperature, the precipitate was removed by filtration. The solvent was evaporated by a rotary evaporator, the crude product was purified by column chromatography using toluene as eluent, and finally 2.18 g white solid was obtained. Yield: 61%. M2 was characterized by FT-IR, NMR, and HRMS (Figure S9, Figure S10, Figure S11, and Figure S12). FT-IR (KBr, cm^{-1}): 2925(-CH_2-), 1630, 1589, 1486(C = C), 1453(-CH_3), 1333 (C-N). ^{1}H NMR (400 MHz, CDCl$_3$) δ 8.13 (d, J = 7.7 Hz, 2 H), 7.58 ~ 7.18 (m, 6 H), 4.36 (t, J = 6.9 Hz, 2 H), 3.39 (t, J = 6.5 Hz, 2 H), 2.17 ~ 2.01 (m, 2 H), 1.98 ~ 1.85 (m, 2 H). ^{13}C NMR (100 MHz, DMSO-d_6) δ 140.38, 126.15, 122.50, 120.74, 119.17, 109.70, 41.82, 35.17, 30.29, 27.69. HRMS(ESI) calcd. for [M + H]$^+$ 302.0466, found 302.0542.

2.5. Synthesis of 9-(4-(9 H-carbazol-9-yl)butyl)-3,6-dibromo-9 H-carbazole (M3)

Under nitrogen atmosphere, the M1 (1.296 g, 3.99 mmol) and tetrabutylammonium bromide (0.04 g, 0.12 mmol) were added to 10 mL of toluene. And then NaOH (50 wt %, 8 mL) was added and left to react for 30 min. M2 (1.2 g, 3.97 mmol) was slowly added by an addition funnel, and the reaction was refluxed for 16 hours. After filtration and removal of the solvent by a rotary evaporator, the residue was purified by column chromatography using toluene as eluent. The final product was obtained as a white solid (1.40 g, 64%). Yield: 61%. M3 was characterized by FT-IR, NMR, and HRMS (Figure S13, Figure S14, Figure S15, and Figure S16). FT-IR(KBr, cm^{-1}): 2926, 2857(-CH_2-), 1350, 1323, 1186, 1056(C-N), 562 (C-Br). ^{1}H NMR (400 MHz, DMSO-d_6) δ 8.45(s, 1H), 8.12 (d, J = 7.7 Hz, 1H), 7.60 ~ 7.45(m, 3 H), 7.40(dd, J = 11.2, 4.0 Hz, 1H), 7.17(t, J = 7.3 Hz, 1H), 4.35(d, J = 5.7 Hz, 2H), 1.80(s, 2 H). ^{13}C NMR(100 MHz, DMSO-d_6) δ 139.88, 138.99, 128.81, 125.64, 123.45, 122.91, 122.00, 120.27, 118.68, 111.71, 111.31, 109.24, 42.25, 41.88, 25.90. HRMS(ESI) calcd. for [M + H]$^+$ 547.0129, found 547.0210.

2.6. Synthesis of poly[(9,9-dioctyl)-2,7-fluorene-co -4,4',4"-triphenylamine-co-9-(4-(9H-carbazol-9-yl) butyl)-3,6-carbazole](P)

Under nitrogen atmosphere, tribromotriaaniline (0.0145 g, 0.03 mmol), R4 (0.271 g, 0.5 mmol), M3 (0.249 g, 0.45 mmol) were added in toluene (8 mL) and then 0.2 M potassium carbonate aqueous solution (1.5 mL). Three drops of Aliquat 336 and Pd(OAc)$_2$ (0.003 g, 0.013 mmol) were added. The above mixture was degassed several times and tricyclohexylphosphine (0.006 g, 0.021 mmol) was added afterwards. The reaction mixture was refluxed for 72 hours under nitrogen

atmosphere before it was cooled to room temperature. The crude product was reprecipitated into methanol, and the formed precipitate was purified by flash column chromatography using toluene as eluent. After purification, it was dried in a 50°C vacuum drying oven overnight to obtain a light green filamentous polymer (111 mg, 30%). FT-IR(KBr, cm^{-1}): 2927, 2850(-CH_2-), 1353, 1141(C-N), 1601, 1466(C = C), 800, 828(C-H). ^{1}H NMR(400 MHz, CDCl$_3$) δ 8.532 ~ 8.455(m, 2.48 H), 8.327 ~ 8.282(m, 1.22 H), 8.157 ~ 8.058(m, 4.30 H), 7.881 ~ 7.602(m, 18.28 H), 7.525 ~ 7.278(m, 14.46 H), 7.139 ~ 7.069(m, 1.12 H), 4.374 ~ 4.165 (m, 8.00 H), 2.212 ~ 1.957(m, 17.38 H), 1.355 ~ 0.889 (m, 55.67 H), 0.820 ~ 0.768 (m, 14.25 H, alky lH).

3. Results and discussion

3.1. Synthesis and characterization

The synthetic route toward poly[(9,9-dioctyl)-2,7-fluorene-co-4,4',4"-triphenylamine-co-9-(4-(9H-carbazol-9-yl)butyl)-3,6-carbazole](P) is depicted in Scheme 1. P was obtained via the Suzuki coupling reaction. P has good solubility in common organic solvents, such as CHCl$_3$, CH$_2$Cl$_2$, toluene, and THF. Results of polymer properties measured by GPC are shown in Table 1. The number-averaged molecular weight (M_n) of P was evaluated by gel-permeation chromatography (GPC) analysis, to be24902g/mol and with a polydispersity index (PDI) of 1.329.

The chemical structures of P were characterized by FT-IR and ^{1}H NMR characterization. As shown in Figure S17, it can be found that the absorption peak at ~1141 cm^{-1}, corresponds to the stretching movement of the (C-N) group in tertiary amine. ^{1}H NMR spectrum of P was shown in Figure S18. It can be seen that the aromatic hydrogen proton peaks of the fluorene, carbazole, and triphenylamine groups appeared at ~ δ 8.523 ~ 7.069 ppm. Chemical shifts within the range of δ 4.374 ~ 4.165 ppm corresponded to the signal of the methylene (-CH_2-), which was connected to the nitrogen of the carbazole. The chemical shifts range from δ 2.212 to 1.957 ppm corresponded to the hydrogen -CH_2- in the fluorine and the hydrogen in the β-methylene group connected to the nitrogen of the carbazole. It can be seen that the ^{1}H NMR spectrum of P matches well with its chemical structure.

3.2. Thermal properties

In order to study the thermal stability of P, the thermo-gravimetric measurement of polymer probe P was conducted in the temperature range from 300 K to 650 K. As
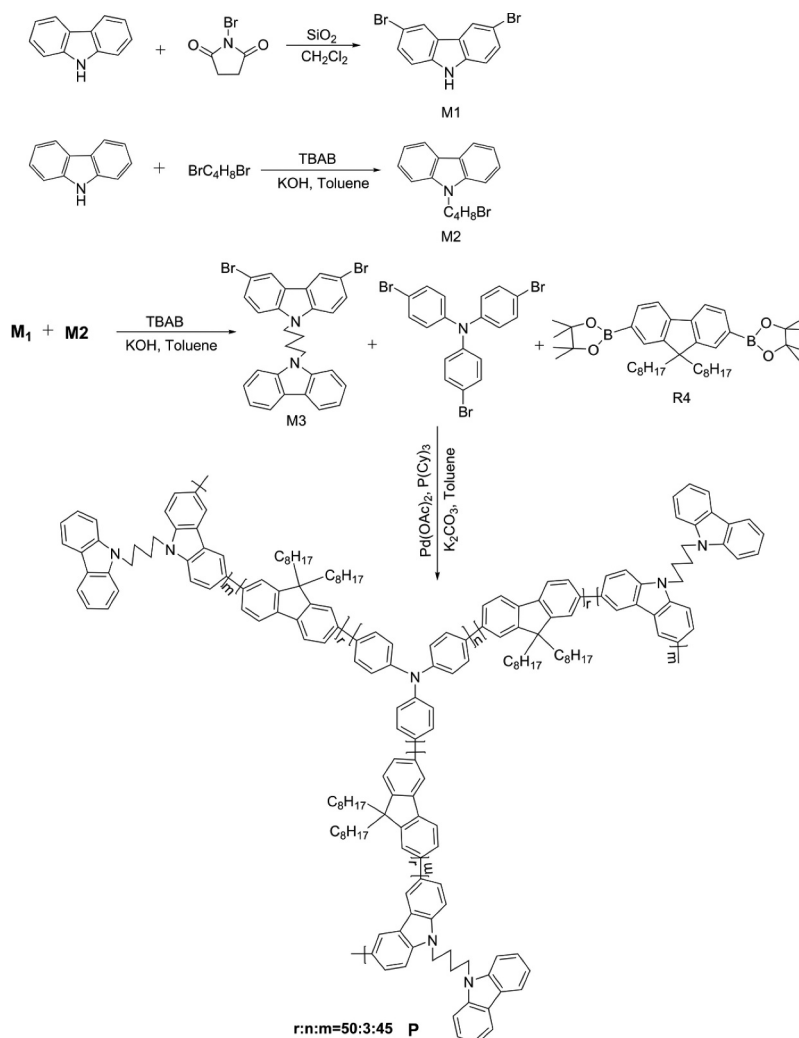
Scheme 1. Synthesis of monomers and polymer.

Table 1. Polymer characterization results determined by GPC.

Mn	Mw	Mp	Mz	PDI	Mz/Mw
24,902	33,107	29,244	44,250	1.329	1.337

Table 2. Comparison of the present method for sensing of I^- with reported methods.

Optical probe	Linear range (μM)	LOD (M)	Ref.
Quinoline-based derivative	0–7	5.48×10^{-8}	[17]
Green-emission carbon dots/Hg^{2+}	0–60	5.0×10^{-7}	[18]
Triphenylamine-based CP	0.8–35	2.3×10^{-7}	[42]
Triazole and Cz-containing CP	0–1.5	2.0×10^{-7}	[43]
Blue-emission carbon dots/Hg^{2+}	0–160	1.0×10^{-6}	[54]
Oligonucleotides	0.02–0.20	5.0×10^{-9}	[55]
Gold nanoclusters	0.01–0.8	1.1×10^{-9}	[56]
Hydrazone derivative	0–10	1.1×10^{-6}	[57]
Tannic-acid-protected Cu-nanoclusters	20–100	1.8×10^{-9}	[58]
Dendritic Carbazole-Based CP	1.48–4.59	6.2×10^{-8}	This work

shown in Figure 1, by analyzing the thermogravimetric test curve of P, it could be found that polymer P began to decompose near 555 K and the structure began to fracture. This indicated that polymer P is stable enough before 555 K, which proves that the probe has good thermal stability.

3.3. Optical response of P toward I^-

To explore the selectivity of polymer P to I^-, spectral response tests of P (with the concentration of ~1.0 × 10^{-5}M in THF) toward common anions were investigated. Figure 2a is the UV-*vis* absorption spectra of P in various common anions. As can be seen from Figure 2a, the absorption peak at 350 nm was significantly enhanced and the color of the solution changed from colorless to light yellow after I^- was

Table 3. Comparison of the present method for sensing of Hg^{2+} with reported methods.

Optical probe	Linear range (μM)	LOD (M)	Ref.
Quinoline-based derivative/I⁻	0–7	3.12×10^{-9}	[17]
Green-emission carbon dots	0–50	8.9×10^{-7}	[18]
Rhodamine-containing CP	10–50	1.07×10^{-8}	[27]
Triphenylamine-based CP/I⁻	0–7	1.1×10^{-7}	[42]
Triazole and Cz-containing CP/I⁻	0–10	1.23×10^{-7}	[43]
Blue-emission carbon dots	0–40	9.0×10^{-7}	[54]
Triphenylamine-bodipy derivative	0–7.5	2.24×10^{-7}	[59]
Naphthalimide derivative	0.25–10	4.0×10^{-8}	[60]
Coumarin derivative	1–6	2.2×10^{-7}	[61]
Dendritic Carbazole-Based CP/I⁻	0.005–14.75	9.7×10^{-8}	This work

Figure 1. Thermal weight curves of P.

added, while other anions have little change. Figure 2b is the fluorescent emission spectra of P in various common anions. Also, it can be seen that the fluorescent intensity was significantly quenched when I⁻ was added and other anionic ions just brought slight influence change.

The concentration titration experiments were also carried out. Figure S3 showed the UV-*vis* absorption spectra of P in the THF solution with the addition of I⁻. As shown in Figure S3, the UV-*vis* absorption spectra of P showed a monotonous increasing trend when the I⁻ concentration was changed from 3.3×10^{-7} M to 3.7×10^{-4} M. When the I⁻ concentration reached 3.7×10^{-4} M, the UV-*vis* absorption spectra almost reached maxima. Figure S4 displayed the detailed fluorescent response of P toward I⁻. With the addition of I⁻, the fluorescent polymer P solution was quenched. The mechanism of fluorescence quenching in this experiment might be via 'heavy-atom' effect between the excited state of carbazole group and I⁻ [40–43]. As can be seen from the illustration in Figure S4, it has a good linear relationship between polymer probe P and iodine ion concentration. The calculated detection limit of P to I⁻ reached 6.2×10^{-8} M by 3σ rule [53].

Response times of I⁻ toward P were carried out, and the corresponding results are shown in Figure 3. It can be seen from Figure 3 that the fluorescent intensity of the P solution reached maxima after adding I⁻in 60 s. It showed that the detection of I⁻ took place immediately. Competition experiments were also investigated, and the results are shown in Figure 4. It can be seen that other coexisting anions have little effect on the detection of probe P. When I⁻ coexisted with these anions, the fluorescence was obviously quenched, which proved that P has excellent anti-interference for I⁻ detection.
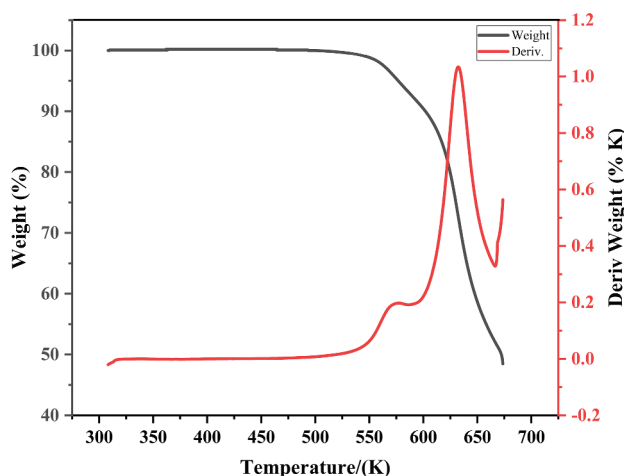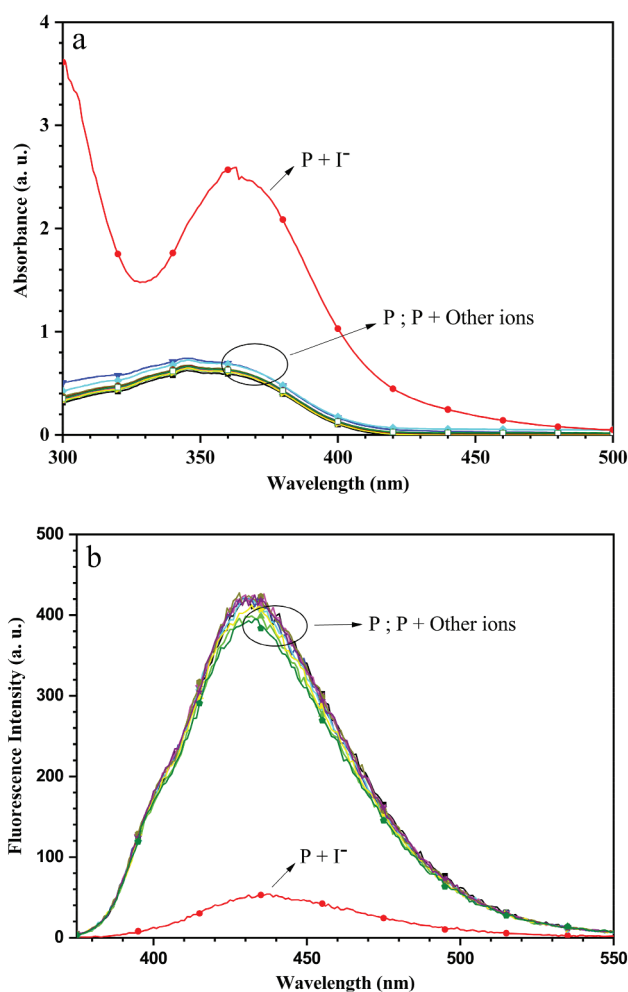
Figure 2. (a) The UV-*vis* spectra of P(THF, 1×10^{-5} M) solution with the addition of different ions(1.32×10^{-4} M). (b) The fluorescence spectra of P (THF, 1×10^{-5} M) with the addition of different ions (1.32×10^{-4} M).
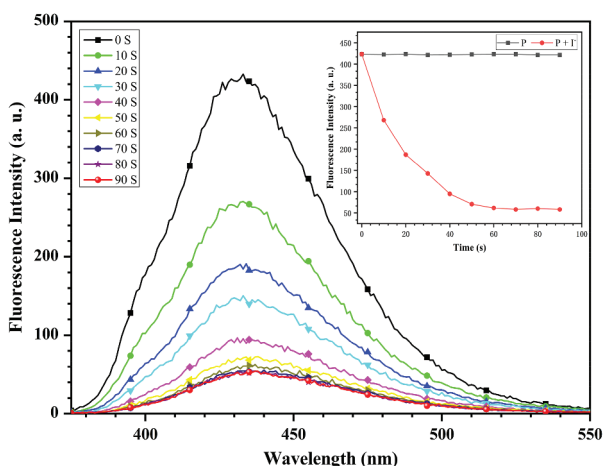
Figure 3. Response time fluorescence spectra of P (THF, 1×10^{-5} M) to I$^-$ (1.32×10^{-4} M), inset was the time response curve of P to I.

3.4. Optical response of P/I$^-$ composite probe to Hg^{2+}

Since I$^-$ and Hg^{2+} have a strong binding effect, it is interesting to explore whether Hg^{2+} was added to the polymer P/I$^-$ system to achieve changes in absorption and fluorescence intensity. Figure 5 shows the UV-*vis* spectra of various metal ions added to the P/I$^-$ system. As can be seen that after adding Hg^{2+} to the P/I$^-$ system, the UV-*vis* absorption was significantly reduced. Meanwhile, the UV-*vis* absorption was only slightly reduced with the addition of Ag$^+$. When other cations were added, the color of the polymer P/I$^-$ solution

remained unchanged. It can be seen from Figure 6 that except Hg^{2+} can restore the fluorescence of the composite system, other ions have no effect on the probe, which indicated the composite probe of P/I$^-$ was feasible for Hg^{2+} detection with the naked eye.

Figure 7a shows the fluorescent emission spectra of probe P after Hg^{2+} stepwise titration. As shown in Figure 7a, when the concentration of Hg^{2+} is (2.95×10^{-4} M), the recovery of the fluorescent intensity has been slowed, and the fluorescent intensity has returned to 78% of the initial value. When Hg^{2+} was dropped again, the fluorescent intensity was almost unchanged. The reason for this could be that the fluorescent quenching groups of HgI$_2$ and [HgI$_4$]$^{2-}$ existed in the polymer system [41–43]. After applying the *3σ* rule [53], the calculated detection limit of the polymer P/I$^-$ system for Hg^{2+} was 9.7×10^{-8} M (Figure 7b).

In order to explore the anti-interference properties of the polymer P/I$^-$ composite probe, the anti-interference experiment of the polymer P/I$^-$ composite probe against Hg^{2+} under background ions was carried out. As shown in Figure 8, P/I$^-$ only showed a strong recognition response to Hg^{2+}, after addition of Hg^{2+} to the polymer P/I$^-$in the presence of other background ions, the fluorescent intensity of the polymer P/I$^-$ could almost be restored, so the polymer P/I$^-$ composite probe has a good detection for Hg^{2+} with anti-interference.

The time response experiment of P/I$^-$ toward Hg^{2+} was also studied. As shown in Figure 9, the time response properties were detected by fluorescence spectroscopy. The intensity of the composite probe P/
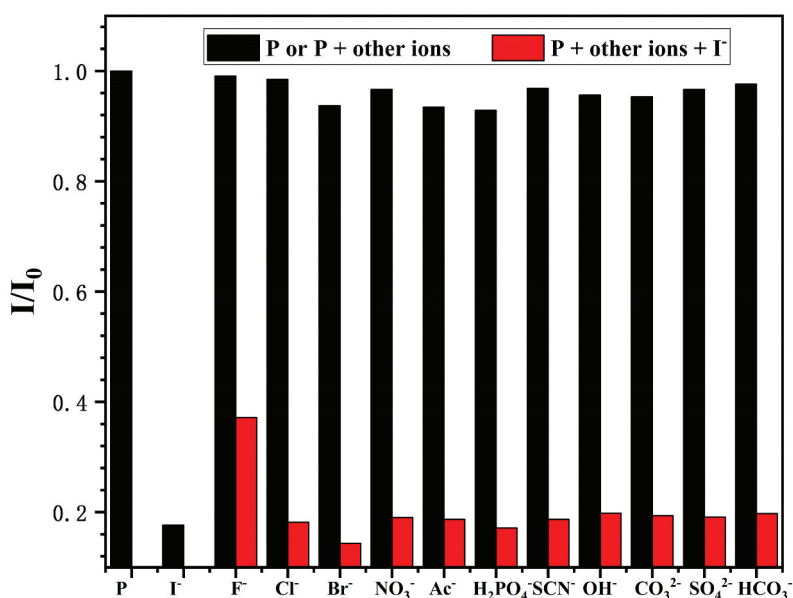

Figure 4. Fluorescence alteration of P in THF(with the concentration of 1×10^{-5} M) in the presence of different background ions (1.32×10^{-4} M) and with sequential addition of I$^-$ (1.32×10^{-4} M).
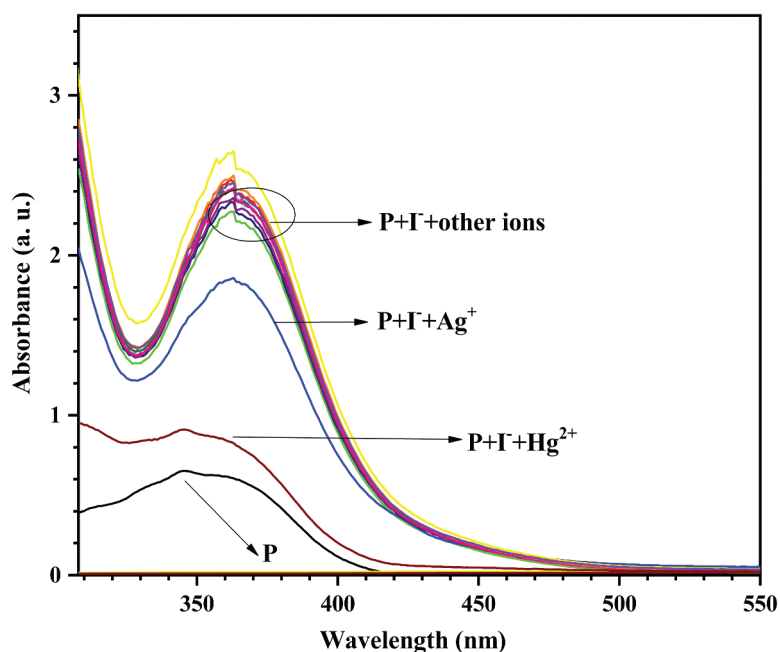
Figure 5. The UV-*vis* spectra of the composite system P/I$^-$ (P: 1 × 10^{-5} M; I: 1.32 × 10^{-4} M) in the presence of different metal cations (8.25 × 10^{-5} M).
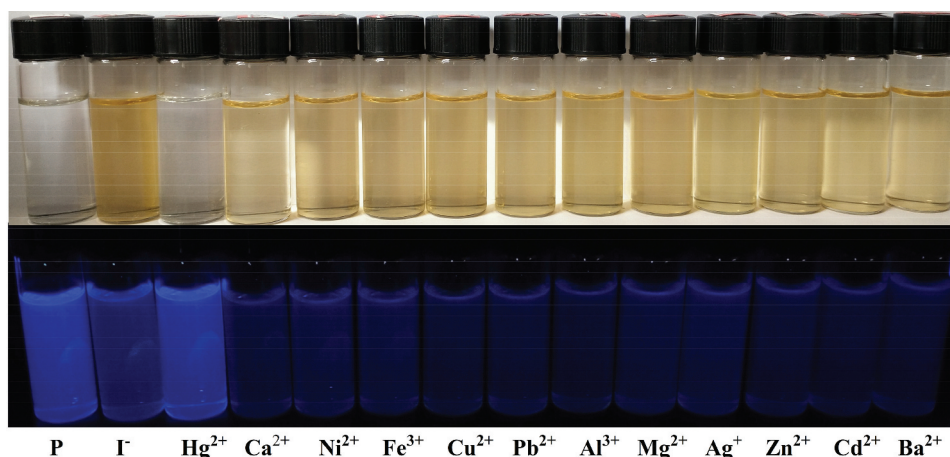

Figure 6. Photograph of P/I$^-$in THF (concentrations of P and I$^-$ were 1.0 × 10^{-5} and 1.32 × 10^{-4} M, respectively) under natural light (upper) and ultraviolet light (365 nm) (bottom) with the addition of various metal ions (8.25 × 10^{-5} M).

I$^-$ was basically stable within 1 min. As Hg^{2+} was added to the probe system, the fluorescent intensity increased gradually after a period of time, and reached stability after 3 min. This showed that P/I$^-$ has good timeliness and is conducive to real-time detection.

The reversible cycle detection of P was investigated. It was found that the polymer probe P showed good reversible cycling in the first 12 cycles due to the alternating introduction of I$^-$ and Hg^{2+}(as is shown in Figure 10). However, with the continuous addition of I$^-$ and Hg^{2+}, the recovery of fluorescent intensity of

polymer probe P was decreasing due to the increasing accumulation of HgI$_2$ or [HgI$_4$]$^{2-}$, which are quenching groups in the system.

Active materials-based test strip experiments were also carried out and represented practical utilization. The filter paper was soaked in the solution of P (1.0 × 10^{-5} M) for a few seconds and dried naturally and the corresponding detection experiments were carried out. The pre-treated filter paper was then exposed to the solution of I$^-$ (0.1 M), and the fluorescent quenching of the test strip could be observed by naked eyes (as
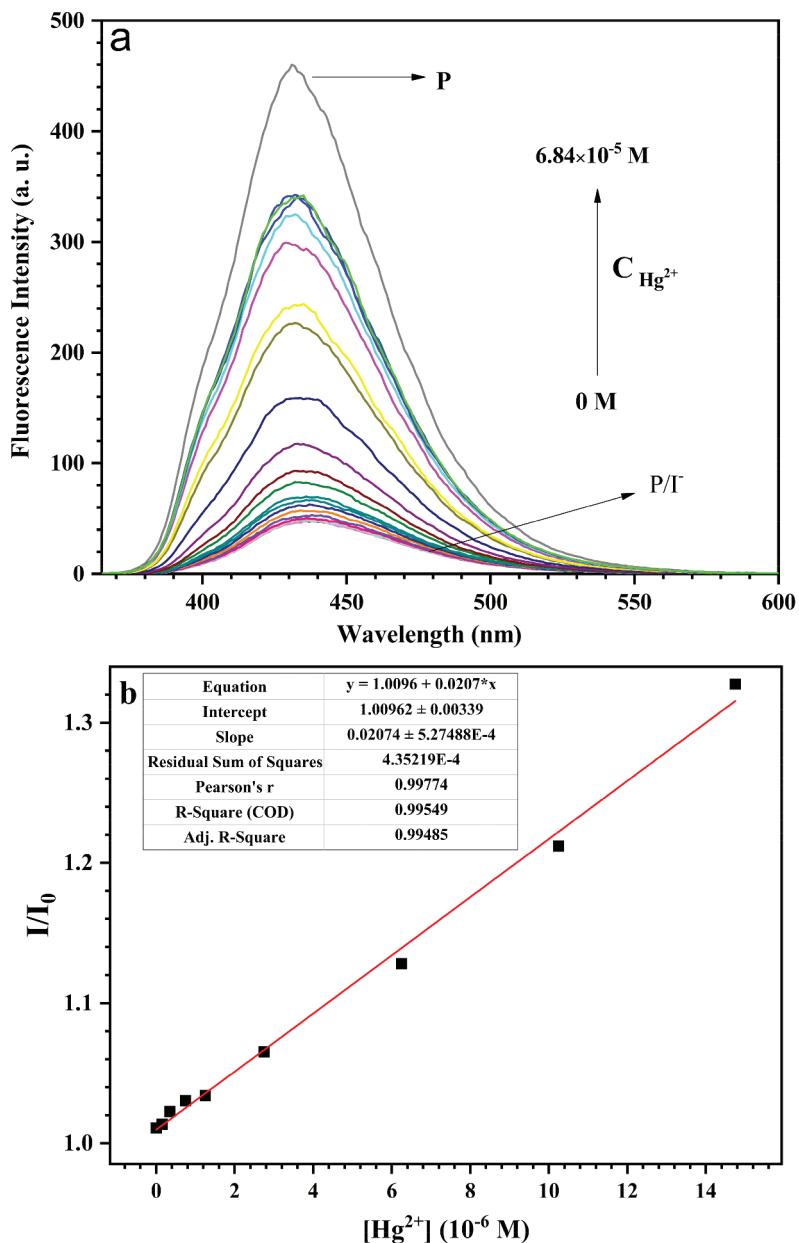
Figure 7. (a) Fluorescence spectra of P/I$^-$ with the addition of Hg^{2+} (concentrations of P and I$^-$ were 1.0×10^{-5} and 1.32×10^{-4} M, respectively) . (b) Calibration curve for the quantification of Hg^{2+} using P/I$^-$ composite (The linear range of the graph was 0.005–14.75 μM).

is shown in Figure 11). When the I$^-$exposed test strip was immersed into the Hg^{2+} (0.01 M) solution, the fluorescent intensity increased significantly. This indicated that the conjugated polymer probe could be expected to be used in practice. The analytical performance of dendritic carbazole-based CP fluorescence method was compared with the reported methods for the detection of I$^-$ and Hg^{2+} (Tables 2, 3). In contrast, although the linear range fitted for I$^-$in this experimental method was relatively narrow, the linear range fitted for the detection of Hg^{2+} by this method showed a wider linear range than that reported method in the literature [17,42,43,59–61]. The calculated detection limit obtained by this experimental method was inferior to the reported detection method [17,27,55,56,58,60], and better than the reported method [18,42,43,53,54,57,59,61]. This method was comparable with the other analytical techniques [6,7], however, the other analytical techniques required high-cost
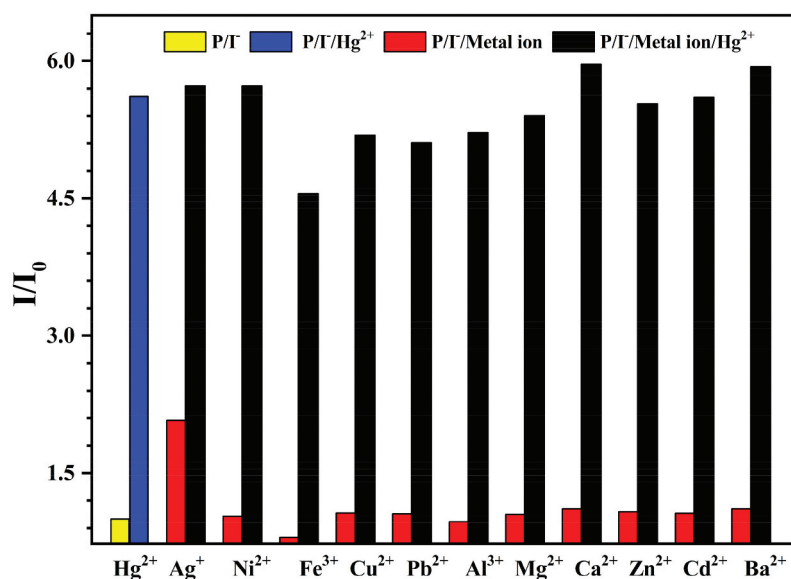
Figure 8. Fluorescence alterations of P/I$^-$ (concentrations of P and I$^-$ were 1.0×10^{-5} and 1.32×10^{-4} M, respectively) in the presence of different background ions(8.25×10^{-5} M) and with sequential addition of Hg^{2+} (8.25×10^{-5} M).
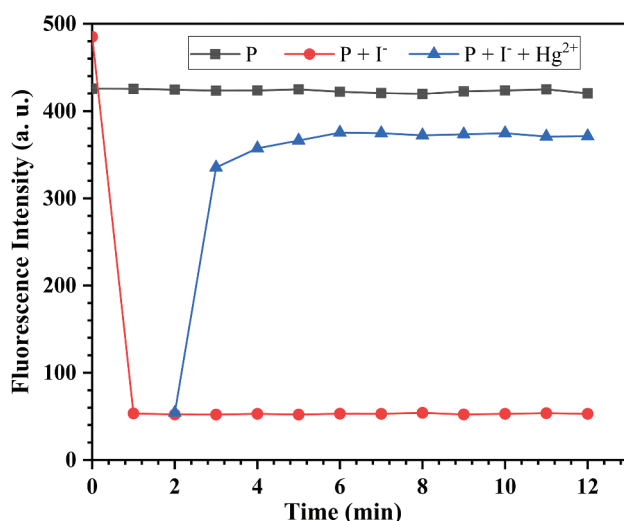

Figure 9. Time response of P/I$^-$ (concentrations of P and I$^-$ were 1.0×10^{-5} and 1.32×10^{-4} M, respectively) to Hg^{2+} (8.25×10^{-5} M).
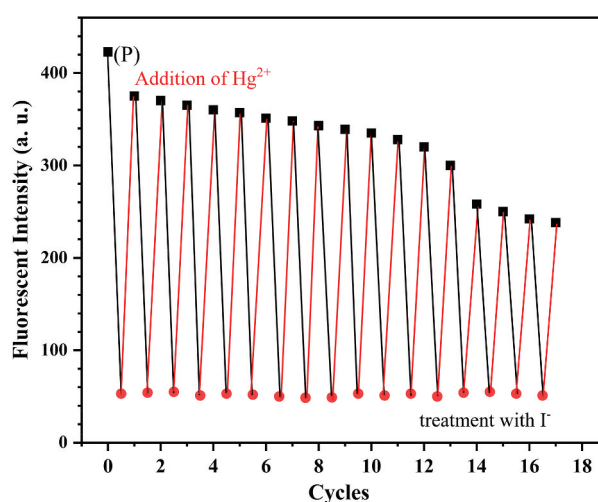
Figure 10. Fluorescence intensity of the probe system with the alternating addition of I$^-$ and Hg^{2+}(P: 1×10^{-5} M; I: 1.32×10^{-4} M, Hg^{2+}: 8.25×10^{-5} M).

instruments, professional operation, extensive sample pretreatment, inevitably rendering them unsuitable for real-time and in the field detection of I$^-$ and Hg^{2+}.

3.5. Theoretical studies

In order to explore the detection mechanism of probe P, ORCA quantum chemistry software was used for electron DFT calculations. The corresponding orbit and energy level diagram and electron hole diagram are shown in Figure 12. Through B3LYP calculation, the

energy level gap between HOMO and LUMO of structural unit of P before the addition of I$^-$ was 4.216 eV, and the energy and oscillator strength of S$_0$ to S$_1$ transition in S$_1$ stable structure were 3.585 eV and 0.06, respectively. Considering the influence of the spin-orbit coupling on fluorescence, it was found that there was no obvious coupling between S$_1$ and T$_X$, and the oscillator strength was 0.0618. After adding iodine ion, the energy gap was 3.565 eV, and the energy and oscillator strength of S$_0$ to S$_1$ transition in S$_1$ stable structure were 2.898 eV and 0.01, respectively. In terms of oscillator strength, after adding of I$^-$, the
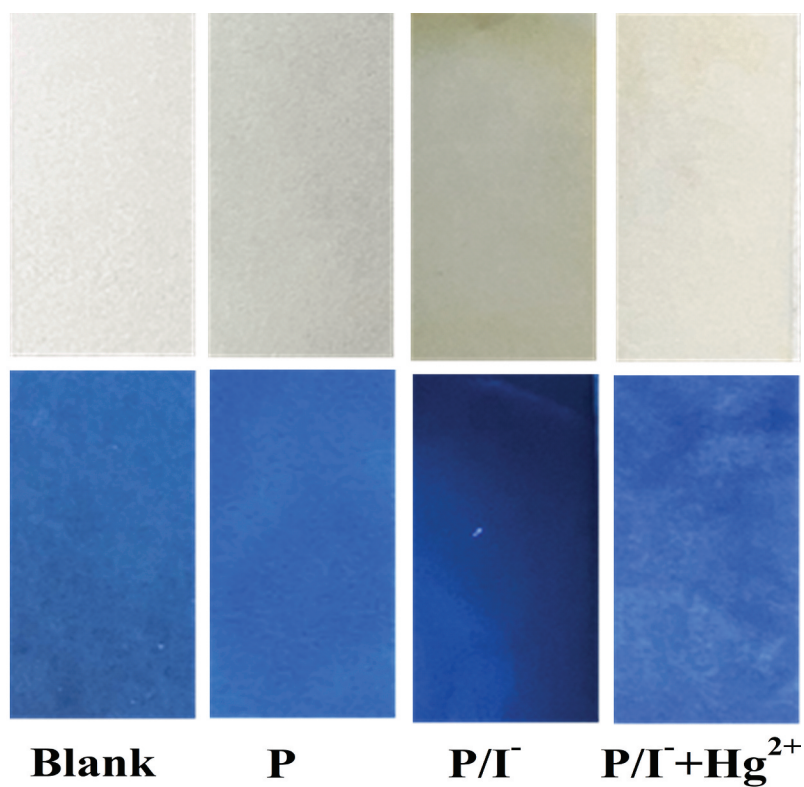
Figure 11. Photographs of filter paper strips: pristine state, immersion of P (10^{-5} M), after addition of I^- (0.1 M), and treated by Hg^{2+} (0.01 M), under natural light (upper) and ultraviolet light (365 nm) (bottom), respectively.
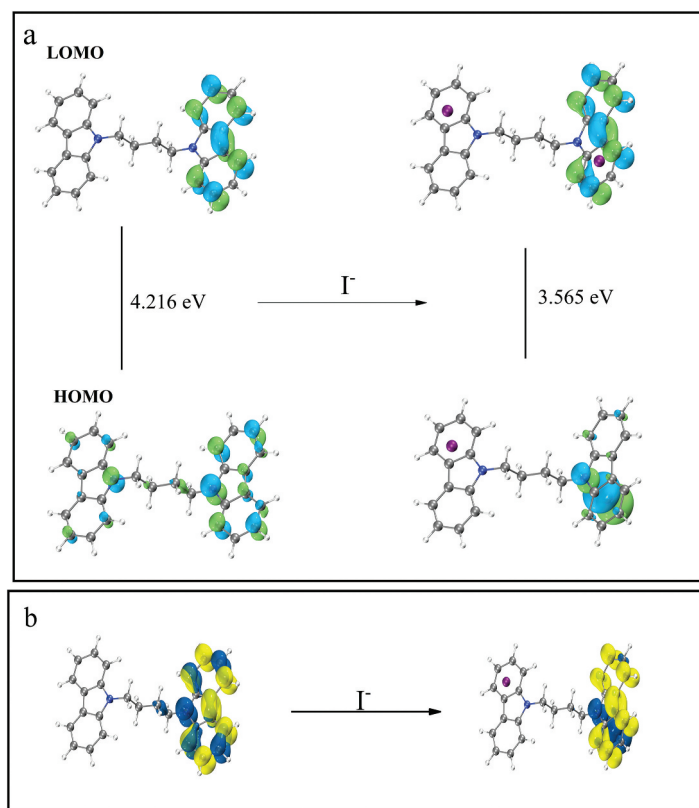

Figure 12. (a) HOMO and LOMO orbital diagrams of structural unit of P before and after dropping I^-. (b) Electron-hole diagrams of structural unit of P before and after dropping I.

fluorescent emission intensity of the system decreased to one-sixth of the original fluorescent intensity, and the oscillator strength has been reduced to the quenching level. This was consistent with our experimental values.

4. Conclusions

A new type of carbazole-based blue-emitting dendritic conjugated polymer P was successfully synthesized by the Suzuki coupling reaction and P showed good thermal stability before 555 K. Optical experiments showed that the polymer has specific selectivity, high sensitivity, and good anti-interference to I^-. Meanwhile, P/I^- complex can achieve the turn-on detection of high toxic Hg^{2+}. The calculated detection limit of I^- and Hg^{2+} can reach 6.2×10^{-8} M and 9.7×10^{-8} M, respectively. Theoretical calculations were in agreement with the experimental data. Test strip experiments indicated that the conjugated polymer probe was expected to be used in practice. P was expected to be a potential optical probe material for two channel cyclic detections of I^- and Hg^{2+}.

Acknowledgments

Disclosure statement

No potential conflict of interest was reported by the author(s).

Funding

References

[1] Harris HH, Pickering IJ, George GN. The Chemical Form of Mercury in Fish. Science. 2003;301(5637):1203.

[2] Jarup L. Hazards of heavy metal contamination. Brit Med Bull. 2003;68(1):167–182.

[3] Bradley MA, Barst BD, Basu N. A review of mercury bioavailability in humans and fish. Int J Environ Res Public Health. 2017;14(2):169–189.

[4] Yoon S, Albers AE, Wong AP, et al. Screening mercury levels in fish with a selective fluorescent chemosensor. J Am Chem Soc. 2005;127(46):16030–16031.

[5] Que EL, Domaille DW, Chang CJ. Metals in neurobiology: probing their chemistry and biology with molecular imaging. Chem Rev. 2008;108(5):1517–1549.

[6] Sardans J, Montes F, Peñuelas J. Determination of As, Cd, Cu, Hg and Pb in biological samples by modern electrothermal atomic absorption spectrometry. Spectrochimica Acta B. 2010;65(2):97–112.

[7] Benipal G, Harris A, Srirajayatsayai C, et al. Examination of Al,As,Cd,Cr,Cu,Fe,Mg,Mn,Ni,Pb,Sb,Se,V, and Zn in sediments collected around the downtown Houston, Texas area, using inductively coupled plasma-optical emission spectroscopy. Microchem J. 2017;130:255–262.

[8] Khun NW, Liu E. Linear sweep anodic stripping voltammetry of heavy metals from nitrogen doped tetrahedral amorphous carbon thin films. Electrochim Acta. 2009;54 (10):2890–2898.

[9] Song F, Yang C, Shao X, et al. A reversible "turn-off-on" fluorescent probe for real-time visualization of mercury-(II) in environmental samples and its biological applications. Dyes Pigm. 2019;165:444–450.

[10] Yarur F, Macairan JR, Naccache R. Ratiometric detection of heavy metal ions using fluorescent carbon dots. Environ Sci-Nano. 2019;69(4):1121–1130.

[11] Liu X, Wang L, Zhang N, et al. Ratiometric fluorescent silver nanoclusters for the determination of mercury and copper ions. Anal Methods. 2015;7(19):8019–8024.

[12] Shi G, Shahid MA, Yousuf M, et al. A "turn-on" fluorescent probe for the detection of permanganate in aqueous media. Chem Commun. 2019;55(10):1470–1473.

[13] Xue SS, Xie ZF, Wen YP, et al. Highly selective and sensitive sulfonylhydrazone type fluorescent probe for rapid detection of mercury(II) and its application in logic gate and adsorption. ChemistrySelect. 2021;6(28):7123–7129.

[14] Shumin SM, Feng DD, Dandan GQ. A dual-channel probe with green and near-infrared fluorescence changes for in vitro and in vivo detection of peroxynitrite. Anal Chim Acta. 2019;1054:137–144.

[15] Mehta VN, Desai ML, Basu H, et al. Recent developments on fluorescent hybrid nanomaterials for metal ions sensing and bioimaging applications: a review. J Mol Liq. 2021;333:115950.

[16] Desai ML, Basu H, Saha S, et al. Fluorescence enhancement of bovine serum albumin gold nanoclusters from La^{3+} ion: detection of four divalent metal ions (Hg^{2+}, Cu^{2+}, Pb^{2+} and Cd^{2+}). J Mol Liq. 2021;336:116239.

[17] Gharami S, Aich K, Ghosh P, et al. A "on-off-on"fluorescent switch for the selective andSequential detection of Hg^{2+} and I^- with applications in imaging using human AGS gastric cancer cells. Dalton T. 2020;49(1):187–195.

[18] Hao XL, Pan XH, Gao Y, et al. Facile synthesis of nitrogen-doped green-emission carbon dots as fluorescent off-on probes for the highly selective sensing mercury and iodine ions. J Nanosci Nanotechnol. 2020;20 (4):2045–2054.

[19] Zhu XW, Guo WJ, Li HZ, et al. Synthesis of a novel water-soluble conjugated polyelectrolyte based on polycyclopentadithiophene backbone and its application for heparin detection. Des Monomers Polym. 2014;17(7):624–628.

[20] Yin MY, Zhang CY, Li J, et al. Highly sensitive detection of benzoyl peroxide based on organoboron fluorescent conjugated polymers. Polymers. 2019;11(10):1655–1666.

[21] Jones DR, Vallee R, Levine M. Novel fluorescent fluorene-containing conjugated polymers: synthesis, photophysical properties, and application for the detection of common bisphenols. Synlett. 2018;29(19):2515–2522.

[22] Li ZJ, Guo H, Xu FY, et al. Sensitive monitoring of RNA transcription by optical amplification of cationic conjugated polymers. Talanta. 2019;203:314–321.

[23] Wang XY, Feng QL, Wang L, et al. A novel polythiophene derivative as a sensitive colorimetric and fluorescent sensor for the detection of ATP. Des Monomers polym. 2014;17(1):26–32.

[24] Thomas S, Joly GD, Swager TM. Chemical sensors based on amplifying fluorescent conjugated polymers. Chem Rev. 2007;107(4):1339–1386.

[25] Scrimin P, Prins LJ. Sensing through signal amplification. Chem Soc Rev. 2011;40(9):4488–4505.

[26] Maimaitiyiming X, Shi CJ. Poly(1,4-diethynylphenylene-4,6-pyrimidine)s for fluorescence detection of mercury-(II) ion. Mater Chem Phys. 2020;257:123783.

[27] Choudhury N, Ruidas B, Mukhopadhyay CD, et al. Rhodamine-appended polymeric probe: an efficient colorimetric and fluorometric sensing platform for Hg^{2+} in aqueous medium and living cells. Acs Appl Polym Mater. 2020;2(11):5077–5085.

[28] Zhang Q, Hu YF, Cheng YX, et al. Carbazole-based hole-transporting materials for electroluminescent devices. Synth Met. 2003;137(1–3):1111–1112.

[29] Han CM, Xie GH, Xu H, et al. Towards highly efficient blue-phosphorescent organic light-emitting diodes with low operating voltage and excellent efficiency stability. Chemistry. 2011;17(2):445–449.

[30] Tan S, Yin Y, Chen WZ, et al. Carbazole-based highly solid-state emissive fluorene derivatives with various mechanochromic fluorescence characteristics. Dyes Pigm. 2020;177:108302.

[31] Lei YL, Niu QL, Mi HY, et al. Carbazole-based conjugated polymer with tethered acetylene groups: synthesis and characterization. Dyes Pigm. 2013;96(1):138–147.

[32] Yang L, Feng JK, Ren AM, et al. The electronic structure and optical properties of carbazole-based conjugated oligomers and polymers: a theoretical investigation. Polymer. 2006;47(4):1397–1404.

[33] Zhang K, Chen Z, Yang C, et al. Improving the performance of phosphorescent polymer light-emitting diodes using morphology-stable carbazole-based iridium complexes. J Mater Chem. 2007;17(32):3451–3460.

[34] Wang PN, Sun Y, Li J, et al. Preparation and application of a D-A conjugated electrochromic flexible electrode with side chain carbazole active groups in supercapacitors. New J Chem. 2021;45(38):18472–18481.

[35] Zhou ZY, Guo D, Shinde DB, et al. Precise sub-angstrom ion separation using conjugated microporous polymer membranes. Acs Nano. 2021;15(7):11970–11980.

[36] Liu K, Wei YH, Xu JY, et al. A poly(carbazole-alt-fluorene) π-conjugated polymer bearing thiophenyl benzimidazole: synthesis, characterization and fluorescence recognition of metal ions and cysteine. Polym Int. 2021;70(11):1612–1620.

[37] Giri D, Patra SK. 1,2,3-Triazolyl functionalized thiophene, carbazole and fluorene based A-alt-B type π-conjugated copolymers for the sensitive and selective detection of aqueous and vapor phase nitroaromatics (NACs). J Mater Chem C. 2020;8(41):14469–14480.

[38] Koyuncu S, Hu P, Li ZQ, et al. Fluorene-carbazole-based porous polymers by photoinduced electron transfer reactions. Macromolecules. 2020;53(5):1645–1651.

[39] Li JL, Grimsdale AC. Carbazole-based polymer for organic photovoltaic devices. Chem Soc Rev. 2010;39(11):1689–1690.

[40] Shi W, Ma FD, Hui YH, et al. TCNE-decorated triphenylamine-based conjugated polymer: click synthesis and efficient turn-on fluorescent probing for Hg^{2+}. Dyes Pigm. 2014;104:1–7.

[41] Tian Y, Shi W, Luo JM, et al. Carbazole-based conjugated polymer covalently coated Fe_3O_4 nanoparticle as efficient and reversible Hg^{2+} optical probe. J Polym Sci Part A Polym Chem. 2013;51:3636–3645.

[42] Shi W, Ma FD, Xie ZF. Sulfur-containing, triphenylamine-based red-emitting conjugated polymer/I assembly as turn-on optical probe for mercury(II) ion. Sens Actuat B Chem. 2015;220:600–606.

[43] Wang LY, Fang GP, Ye DC, et al. Carbazole and triazole-containing conjugated polymer as a visual and fluorometric probe for iodide and mercury. Sens Actuat B Chem. 2014;195:572–580.

[44] Yang RQ, Tian RY, Hou Q, et al. Synthesis and optical and electroluminescent properties of novel conjugated copolymers derived from fluorene and benzoselenadiazole. Macromolecules. 2003;36(20):7453–7460.

[45] Neese F. Software update: the ORCA program system, version 4.0. Wiley Interdiscip Rev Comput Mol Sci. 2018;8(1):1–6.

[46] Adamo C, Barone V. Toward reliable density functional methods without adjustable parameters: the PBE0 model. J Chem Phys. 1999;110(13):6158–6170.

[47] Andrae D, Häußermann M, Dolg, H, et al. Energy-adjusted ab initio pseudopotentials for the second and third row transition elements. Theor Chim Acta. 1990;77(2):123–141.

[48] Weigend F, Ahlrichs R. Balanced basis sets of split valence, triple zeta valence and quadruple zeta valence quality for H to Rn: design and assessment of accuracy. Phys Chem Chem Phys. 2005;7(18):3297–3305.

[49] Grimme S, Ehrlich S, Goerigk L. Effect of the damping function in dispersion corrected density functional theory. J Comput Chem. 2011;32(7):1456–1465.

[50] Grimme S, Antony J, Ehrlich S, et al. A consistent and accurate ab initio parametrization of density functional dispersion correction (DFT-D) for the 94 elements H-Pu. J Chem Phys. 2010;132(15):154104–154123.

[51] Barone V, Cossi M. Quantum calculation of molecular energies and energy gradients in solution by a conductor solvent model. J Phys Chem. 1998;102(11):1995–2001.

[52] Aravena D, Neese F, Pantazis DA. Improved segmented all-electron relativistically contracted basis sets for the lanthanides. J Chem Theory Comput. 2016;12(3):1148–1156.

[53] Thomsen V, Schatzlein D, Mercuro DS. Limits of detection in spectroscopy. Spectroscopy. 2003;18(12):112–114.

[54] Hao X, Dai S, Wang J, et al. Synthesis of blue fluorescent carbon dots and their application in detecting mercury and iodine based on "off-on" mode. Luminescence. 2021;36 (3):721–732.

[55] Li Q, Li SH, Chen X, et al. A G-quadruplex based fluorescent oligonucleotide turn-on probe towards iodides detection in real samples. Food Chem. 2017;230:432–440.

[56] Su Z, Wang XY, Luo MC, et al. Fluorometric determination of nitrite through its catalytic effect on the oxidation of iodide and subsequent etching of gold nanoclusters by free iodine. Mikrochim Acta. 2019;186(9):1–7.

[57] Chen J, Lin Q, Li Q, et al. A highly selective colorimetric chemosensor for detection of iodide ions in aqueous solution. Rsc Adv. 2016;6(89):86627–86631.

[58] Cao XL, Li X, Liu FX, et al. Copper nanoclusters as fluorescence-quenching probes for the quantitative analysis of total iodine. Luminescence. 2018;33 (5):981–985.

[59] Shen BX, Qian Y. Triphenylamine-BODIPY fluorescent dendron: click synthesis and fluorometric chemodosimeter for Hg^{2+}, Fe^{3+} based on the C=N bond. Chem Sel. 2017;2(8):2406–2413.

[60] Tian MJ, Wang CY, Ma QJ, et al. A highly selective fluorescent probe for Hg^{2+} based on a 1,8-naphthalimide derivative. Acs Omega. 2020;5 (29):18176–18184.

[61] Xu MS, Wang L, Li M, et al. A new highly sensitive and selective fluorescent probe for Hg^{2+} and its application in living cells. Phosphorus Sulfur. 2021;196(1):13–18.